

Granulation and magnetism in the solar atmosphere^{*}

F. Baudin¹, R. Molowny-Horas¹, and S. Koutchmy²

¹ Instituto de Astrofísica de Canarias, E-38200 La Laguna, Tenerife, Spain

² Institut d'Astrophysique de Paris, CNRS, 98bis Bd Arago, F-75014 Paris, France

Received 28 May 1996 / Accepted 20 May 1997

Abstract. The properties of the photosphere in magnetic and non magnetic regions, at two levels in the solar atmosphere, have been studied, using two virtually simultaneous time sequences of 109 mn duration of CCD images taken at the Vacuum Tower Telescope of the Sacramento Peak Observatory. The selected wavelengths correspond to the true continuum and to the wing of the MgIb₁ line, where brightenings are taken as proxies of magnetic elements. Averaged intensities, intensity fluctuations and horizontal motions in different regions and levels of the photosphere have been compared. We obtained various results concerning: the intensities inside and outside an active region showing different behaviours; the granulation keeping a kind of remnant structure at the continuum level; the mapping of proper motions of the granules imaged in the continuum outlining clearly the super-granular cells in the deepest layers of the photosphere; the “freezing” influence of the magnetic field on these motions in active regions; and the temporal variation of the correlation between images at the two heights indicating that intensity variations at the higher level precede those of the lower one.

These results are briefly discussed and compared with previous ones and with published model calculations.

Key words: Sun: photosphere; granulation; magnetic fields; activity – convection

1. Introduction

A large part of the solar interior energy is transmitted by convection towards the photospheric level, where a small part is stored in concentrated magnetic fields. In the upper atmosphere, the quasi laminar convective flow compete with the more turbulent motion of eddies of different scales. The phenomenon of

granulation is currently being intensively studied (see the conferences of last years: Stenflo 1990, Rutten & Schrijver 1994) so the subject does not need an extensive introduction. However, some important results relevant to our study may be pointed out. In the past, spectrographs and scanning methods with pin hole photometer as well as raster scans with multichannel systems were used to collect precise data. Classical results were reported by Frazier (1970, 1971) who considered both the case of the quiet sun and of plages from precise spectrographic photoelectric measurements. The influence of magnetic phenomena was clearly shown at photospheric levels: a small brightening in the continuum, related to small magnetic regions called “flux tubes”. Later, the photographic experiment SOUP yielded other classical results (Title et al. 1989) showing the influence of 5 mn oscillations on the granulation. The important role of the mesogranulation was outlined in this work, using local correlation technics (November 1986), and also in other works as Koutchmy & Lebecq (1986) using spatial variations of intensity. The problem of granulation is theoretically studied with numerical simulations of the convection to help the interpretation of the observations, as for instance by Chan et al. (1991), or in the most recent work of Gadun (1995). These works predict the evolution of the temperature and of the vertical and horizontal velocities with height. However, these predictions are usually based on models of the granulation which do not include oscillatory motions nor waves. Furthermore, the influence of the magnetic field should be considered, in particular to separate the problems of mass flows due to pure thermal instability from those of magneto-convection. This is specially important since it is well known that the magnetic field is concentrated and the magnetic pressure cannot be neglected in the regions of flux tubes.

A statistical analysis based on well calibrated data, leading to the estimation of the relevant parameters of the granulation, is a valuable approach to tackle these problems. Such analysis must be performed using new observational tools like precise and linear 2D imagers and narrow pass-band spectral filters. Indeed, an important aspect of the measurements is the photometric accuracy (Koutchmy 1994). The use of CCD devices provide photometrically reliable data. However, another impor-

Send offprint requests to: S. Koutchmy

^{*} Based on observations made at the Vacuum Tower Telescope of the National Solar Observatory/Sacramento Peak Observatory (New Mexico, USA)

tant photometric problem is the mixing of the contribution of the lines emission with the contribution of the true continuum formed in the deepest layers. In the optical blue region, the line blocking effect is of the order of 10% in a $\approx 10\text{nm}$ bandwidth, and in network elements, the line brightening is typically of 30% to 50%. Thus, a true continuum window, which means a very narrow region in the optical domain, must be used, implying the use of a very narrow passband filter. Finally, to fully consider the problems connected with the influence of the magnetic field on convection and the occurrence of magnetic elements, the use of imagers is needed in order to discriminate the magnetic regions from the non magnetic ones. It could appear that very high spatial resolution observations is preferable. We do not cover this aspect in this work. We think it is difficult, if not impossible, to simultaneously consider very high spatial resolution images and the removal or the analysis of several phenomena like 5 mn intensity oscillations, meso-granulation and the network cells boundaries which cannot be ignored when the photospheric convection is studied. We will focus this paper on specific parameters related to the granulation field in magnetic and non magnetic regions, at two levels in the solar atmosphere, leaving to another work results pertaining to oscillations at different levels, as well as results on the dynamical properties of higher layers in the chromosphere.

2. Observations, instrumental parameters and set-up

The observations were obtained at the Sacramento Peak Observatory Vacuum Tower Telescope (VTT) on September 18th, 1994, from 15 h 32 mn to 17 h 22 mn UT. The observed region was a square of $350''$ side, centered at N $17^\circ 3'$, E $1^\circ 3'$. The data were acquired using a specially prepared set-up at one of the auxiliary focus of the VTT. After a re-imaging system demagnifying the field of view (FOV), a 1024×1024 pixel CCD camera was placed at the exit of the Universal Bi-refrangent Filter (UBF). Before the UBF, a beam splitter allowed the re-imaging of the field through an H α Zeiss filter (25 pm FWHM). Four images (true continuum and MgIb₁ blue wing, H α red and blue wing) were taken sequentially every 15 s, up to a total of 110 for each wavelength, with the parameters listed in Table 1. The time interval between consecutive images at the same wavelength was therefore 1 mn. The optical setup yielded a spatial resolution at its focal plane of $0''.34$ per pixel. Several sequences of “dark current” and “flat field” were used to correct the raw images in order to reach the high photometric accuracy allowed by the high level of counts (about 25 000 counts per pixel in average). We used only a sub-region of the FOV of 600×600 px to avoid the remaining vignetting after the flat field correction. The bandwidth we used with the UBF (see Table 1) yields true measurements in the continuum, not affected by line brightenings with a precision better than 0.1%.

The very high correlation between magnetogram signal and brightness in the wing of the MgIb₁ line in small scale magnetic field is well known (Beckers 1976, Dara-Papamargaritis & Koutchmy 1983). Moreover, this line is not affected by the cancellation of fields of opposite polarity within the resolution

Table 1. Parameters of the observations for the 4 sequences of images. $\Delta\lambda$ is the spectral FWHM, and Δt the exposure time

λ [nm]	$\Delta\lambda$ [pm]	Δt [s]	Line identification
525.6400	13.5	0.6	True continuum
518.3219	13	1.4	MgIb ₁ blue wing ($\lambda_0 - 40$ pm)
656.3558	21.4	0.8	H α red wing ($\lambda_0 + 75$ pm)
656.2058	21.4	0.8	H α blue wing ($\lambda_0 - 75$ pm)

element, so one can use the MgIb₁ brightness as a very good proxy for small scale magnetic fields. At the wavelength used (see Table 1) the height of formation is approximately 140 km (Stellmacher -private communication- and Stellmacher & Wiehr 1991).

3. Analysis and results

The first step of the analysis is the separation of the “active” region (hereafter “A region”) from the “quiet” region (hereafter “Q region”). The active region is defined using the average image in the MgIb₁ line wing over the whole 109mn time sequence. This image is smoothed using a boxcar window 30 pixels wide (equivalent to approximately $10''$), and then, pixels having an intensity higher than the average are defined to be the region A. The Q region is made of the pixels outside these contours, having intensities lower than the average (see Figs. 1 and 2). However this definition is not sufficient due to the small scale magnetic structure of an active region. A more sophisticated definition is necessary for the A region. Correlograms of intensities in the continuum and in the MgI line are then calculated for the A and Q regions, separately for each pair of images of the temporal sequence (Fig. 3). There, one can see three components in the correlograms for the A region: one is very similar to the distribution of points in the correlogram of the Q region, whereas a second group of points corresponds clearly to the bright points in the MgI image and a third to the pores. The results of the correlogram of the Q region (Fig. 3a) is used to analyse the correlogram of the A region. We divide it in sub-regions:

-firstly, pixels having an intensity in the continuum lower than ($< I_{Cont/Q} > -3\sigma_{Cont/Q}$) are considered as pores. This limit is illustrated by the vertical line in Fig. 3.

-secondly, another separation is needed to discriminate the pixels corresponding to abnormally bright points in the MgI line wing. This limit is defined as the line ($I_{Mg/Q} = \alpha I_{Cont/Q} + 3\sigma_{Mg/Q}$), where α is the linear regression coefficient.

Pixels from A region but not from the pores sub-region and below this second limit will correspond to a region called “active quiet” (hereafter “AQ region”) since they are in the A region but their intensity distribution is similar to that of the pixels of the Q region. Pixels above this level (and not from pores sub-region) will correspond to an “active active region” (hereafter “AA region”) since their abnormally high intensities in the MgI line wing indicate high non-spot magnetic field values. Points with abnormally low intensity in the continuum (pores), will not be taken into account in this analysis. The approximate number

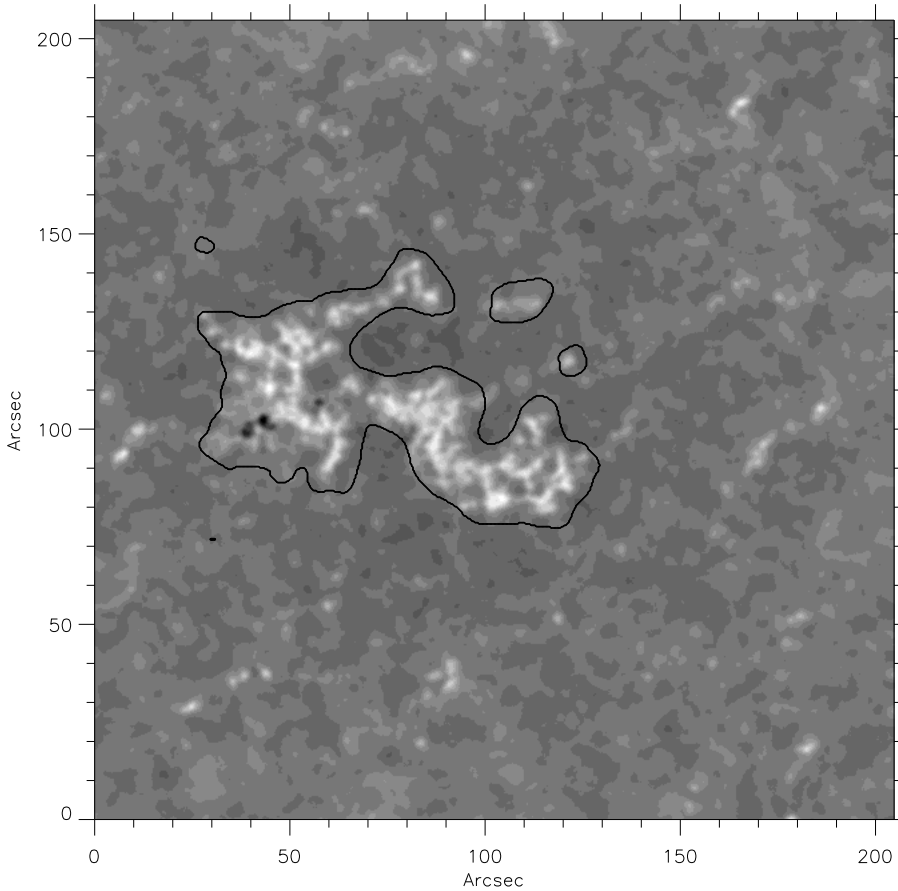


Fig. 1. Image averaged over the 109 mn sequence obtained in the wing of the MgIb_1 line. The A region is defined as the interior of the black contours, while the Q region is the region outside the contours (see text)

of pixels of the Q, AQ and AA regions are respectively: 300000, 20000 and 4000.

3.1. Spatial behaviour of intensity fluctuations

Once the regions are defined, it is possible to calculate some of their statistical characteristics as their mean intensity and their spatial standard deviation, also called σ or RMS. These parameters were computed for each image of the time sequence, yielding an averaged value and its dispersion δ from which we derived errors intervals as the $\pm 3\delta$ range. The mean intensity of each region (Q, AQ and AA) was calculated for the continuum images, and then normalised to the mean intensity in the Q region. The results over the 110 images show (see Table 2) that the AA region is slightly but significantly darker than the Q region at the continuum level, whereas the AQ region is slightly brighter. The spatial standard deviation of intensities were computed as well for these regions, outlining an abnormal granulation in both the AA and AQ region. The same parameters were computed for the images taken in the wing of the MgIb_1 line. It appears that the intensity in the AA region is in average about 12% higher than in the Q region. In order to investigate the influence of acoustic waves on these results, we have employed a so-called “acoustic” filter (see *e.g.* Title et al. 1989 for a thorough description) which allows the separation of the component due to acoustic modes from the rest of

Table 2. Averaged intensities and spatial standard deviation for the Q, AQ and AA regions, computed with no filtered data and subsonically filtered data. For both continuum and MgI line, intensities are normalised by the averaged intensity in the Q region ($\langle I_{Cont/Q} \rangle = 100$ and $\langle I_{Mg/Q} \rangle = 100$)

	Without filtering	Subsonic filter
$\langle I_{Cont/AQ} \rangle$	100.26 ± 0.03	100.30 ± 0.02
$\langle I_{Cont/AA} \rangle$	99.25 ± 0.05	99.56 ± 0.03
$\langle I_{Mg/AQ} \rangle$	102.01 ± 0.06	101.44 ± 0.04
$\langle I_{Mg/AA} \rangle$	113.72 ± 0.47	111.78 ± 0.24
$\langle \sigma_{Cont/Q} \rangle$	2.82 ± 0.17	2.43 ± 0.12
$\langle \sigma_{Cont/AQ} \rangle$	2.54 ± 0.14	2.18 ± 0.10
$\langle \sigma_{Cont/AA} \rangle$	2.67 ± 0.12	2.33 ± 0.09
$\langle \sigma_{Mg/Q} \rangle$	3.48 ± 0.12	2.56 ± 0.05
$\langle \sigma_{Mg/AQ} \rangle$	4.09 ± 0.14	3.08 ± 0.07
$\langle \sigma_{Mg/AA} \rangle$	2.57 ± 0.09	2.75 ± 0.05

the signal. All of the previous parameters have been computed using “subsonically” filtered (p -modes removed) data. Despite changes in absolute value, no relative differences arise from the comparison of the two datasets (see Table 2).

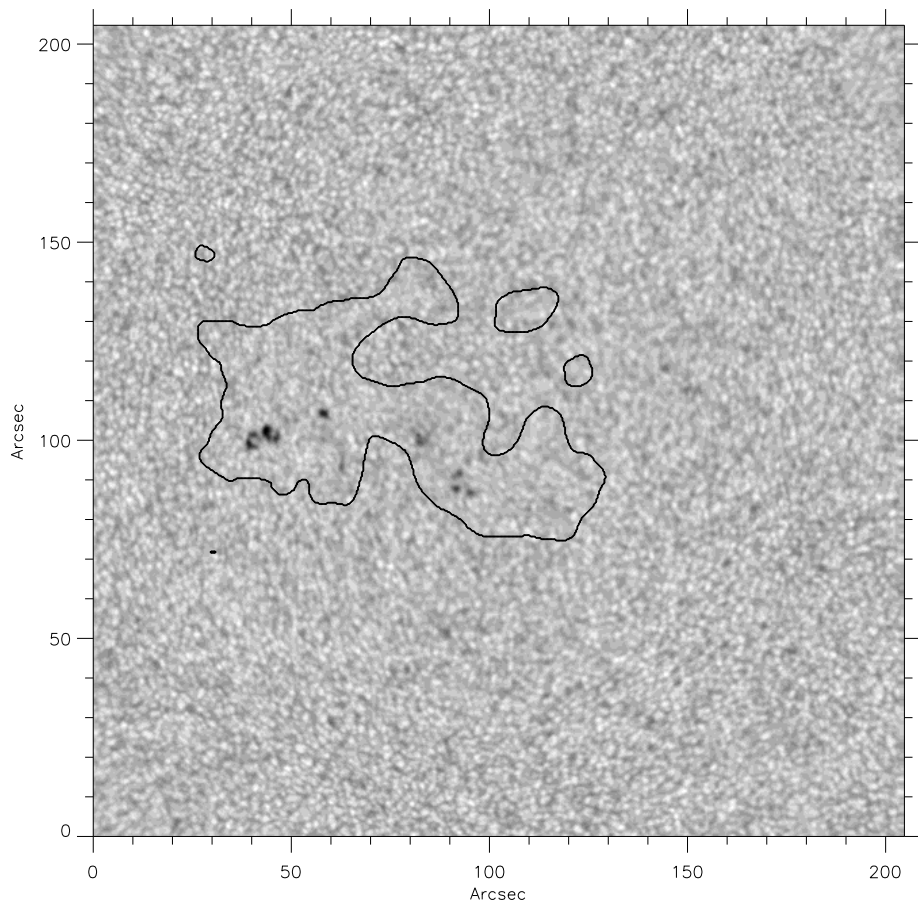


Fig. 2. Sample image of the granulation obtained in the true continuum. The closed contours separate A and Q region, as in Fig. 1

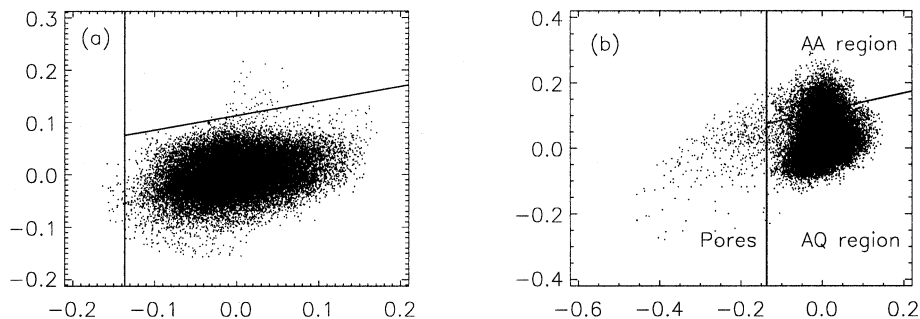


Fig. 3a and b. Correlogram between continuum and MgIb₁ intensities, for a sample pair of images, for the Q region (a) and the A region (b). Dividing lines are the same in a and b

3.2. Intensity correlations

Another important result yielded by this analysis is the spatial correlations in the Q region when the intensities in the MgIb₁ line wing are plotted as a function of the intensities in the continuum. The correlation coefficient C between continuum and MgIb₁ intensities in the Q region for the 110 raw images has an averaged value of $\langle C \rangle = 0.43$, and is always included in the interval $0.32 \leq C \leq 0.53$. In order to investigate the origin of this correlation we made a more detailed study using the three data sets yielded by the acoustic filter: the raw, the subsonically filtered (p -modes signal suppressed) and the supersonically filtered (every but the p -modes eliminated) data sets. The correlation coefficient between continuum and MgIb₁ intensities as a

function of time difference has been computed. Figure 4 shows the three curves (raw, subsonically and supersonically filtered data), which have been averaged for a number of cases. In the three cases, the correlation remains positive. The maximum of the correlation function of the raw images is slightly shifted towards negative values. The correlation function of the supersonic images is symmetric and maximum for a time difference $\Delta T \approx 0$, which is expected since acoustic modes are standing waves, and thus, are well in phase in the whole photosphere. More surprisingly, the correlation of the subsonic filtered images peaks at a negative time difference $\Delta T \approx -2$ mn. This implies that, for the “subsonic” part of the signal, the variations of intensities at the MgIb₁ level precede those at the continuum level. We next carried out a careful analysis of the images, in

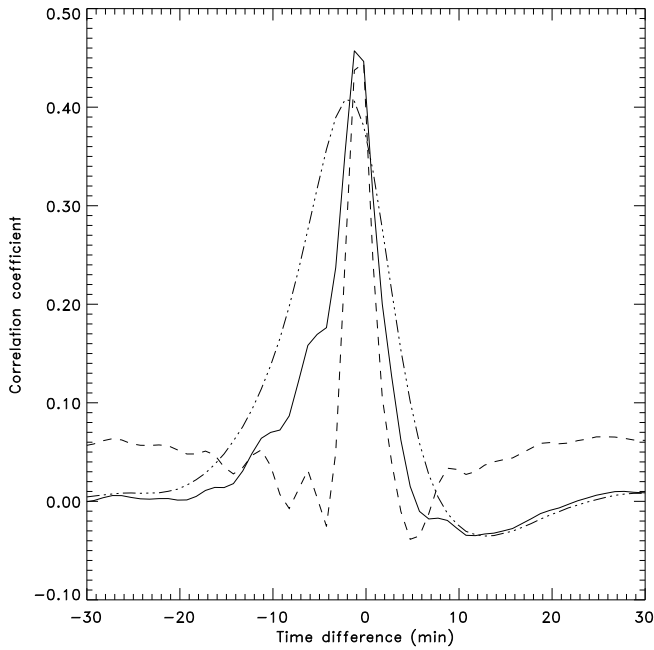


Fig. 4. Mean correlation curves between continuum and MgIb₁ images, as a function of time difference, for original (solid), subsonically filtered (dot-dashed) and supersonically filtered (dashed) images

order to determine the pattern responsible for this correlation. We established that the observed correlation is related to dark structures of spatial scale larger than that of granulation, but we did not draw further conclusion.

It is also worthwhile to compare the RMS of the intensity of single images (SI) with the RMS of the mean image (MI) after averaging over the whole 109 mn time sequence. The RMS value of the averaged image is 1.2%, whereas the RMS of instantaneous images (SI) is on average $\sigma_{SI} = 2.8\%$, illustrated by the fact that a clear pattern subsists in the average image (Fig. 5). The observed decreasing of the RMS from 2.8% to 1.2% should be attributed to the averaging of a succession of independent “realisations” of the granulation pattern. Obviously, the lifetime of the granulation must be accounted for, but this number seems small compared to the duration of the time sequence. Moreover, the spatial correlation of each instantaneous image with the mean image was computed taking into account only the Q region, yielding a mean value of $\langle C_{SI/MI} \rangle = 0.34$, which suggests that there is a persistent, long-lived granulation giving rise to the observed pattern. In order to determine the spatial scale responsible of this correlation, we computed the same correlation using spatially filtered images. The instantaneous images and the averaged one were filtered with different spatial bandpass. The variations of the correlation coefficient versus wavenumber show a maximum between $2Mm^{-1}$ and $4Mm^{-1}$ (Fig. 6), indicating that the spatial scale responsible of the correlation is between 1500 km and 3000 km, which is about the size of the granulation pattern.

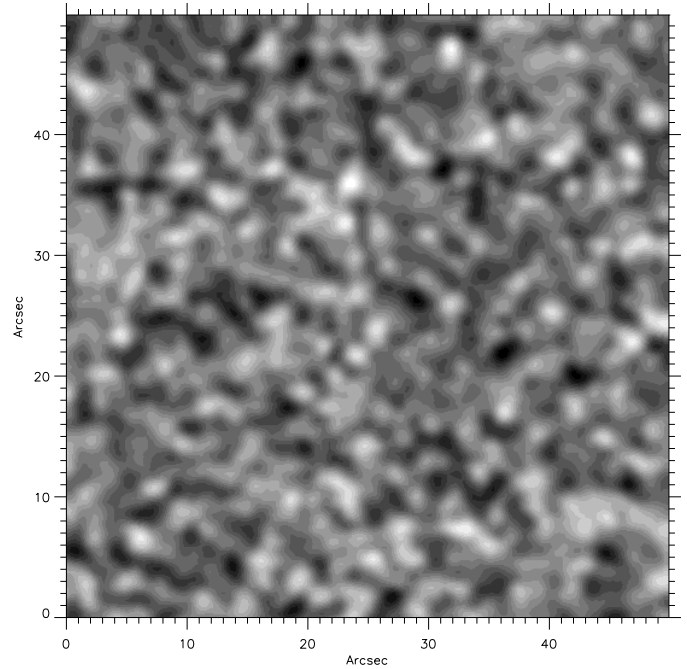


Fig. 5. Blow-up of a quiet region taken in the continuum, after an averaging over the whole time sequence (109mn). The residual RMS of the intensity fluctuations is 1.2%. This should be compared to the average RMS of instantaneous images: 2.8% (see text)

3.3. Horizontal motions

In order to investigate the behaviour of the horizontal velocities versus height in the solar atmosphere, we applied the so-called “local correlation tracking” technique (November 1986, Molowny-Horas & Yi 1994) to both time sequences (continuum and MgIb₁ line). Time separation between correlated images was 1 mn. The resulting averaged correlation function from the 108 image pairs was convolved by a gaussian window with a full width at half maximum of $4.1''$, and then the offset was calculated by a parabolic interpolation. The corresponding “flow” maps are shown in Figs. 8 and 9. The flows at the continuum level outline clearly the supergranulation cells (visible in simultaneous intensity observations in H α wings, see Fig. 10), whereas these cells are not visible at the level of the MgIb₁ line, where structures of smaller spatial scale are identified.

We calculated the average horizontal velocities both in A and Q regions, at the two levels of the atmosphere. In the A region, the average velocities are very similar: $\langle V_{Cont/A} \rangle = 270$ m/s and $\langle V_{Mg/A} \rangle = 280$ m/s, whereas in the quiet region, they increase drastically when going higher up in the atmosphere: $\langle V_{Cont/Q} \rangle = 340$ m/s and $\langle V_{Mg/Q} \rangle = 680$ m/s. This behaviour is illustrated by the histograms of the velocities calculated (Fig. 7). We also computed the correlation between the modulus of the velocity at the two levels. We obtained a correlation coefficient of $C_A = 0.39$ for the A region and $C_Q = 0.18$ for the Q region. We also made these computations using the X and Y components of the velocity vector and we found a cor-

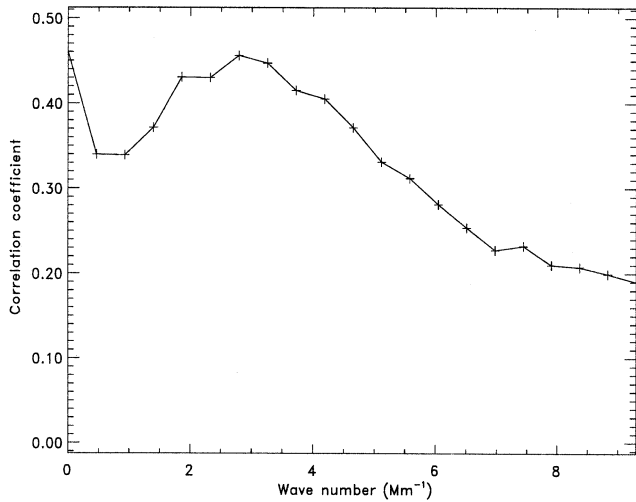


Fig. 6. Correlation between instantaneous continuum images and the time averaged continuum image, as a function of the wavenumber

relation about 0.45 for the Q region and about 0.60 for the A region, which confirms a similar behaviour of the flows when magnetic field is present.

Using the horizontal velocities, we have also studied the motions of the bright points seen in the MgIb₁ images. Some of them exhibit steady proper motions during the 109 mn observing interval. Figure 11 shows three subimages of one bright point during the time sequence. It has moved by ≈ 1450 km after 109 mn, leading to a transversal velocity of 220 m/s. This agrees well with the radial velocity component of intranetwork fields (Wang et al. 1989), as well as with the proper motion of filigrees (Zhang & Engvold 1993). To investigate whether this motion is partly or totally mirroring the horizontal velocity field of the photosphere underneath, a test particle whose initial position coincides with that of the bright point has been allowed to drift during 109mn with the photospheric flow field. The resulting trajectory (Fig. 11) follows very closely that of the bright point. However, one must note that other bright points in the same figure do not display any detectable motion. A close inspection of the whole field of view reveals that out of the fraction of migrating points, all but one move in accordance with photospheric flow field underneath.

4. Discussion

We can firstly discuss the values of the RMS intensity fluctuations we have measured. They are not corrected from any resolution effect (no Modulation Transfer Function correction), but can be compared to previous observations of Keller & Koutchmy (1991). We can confirm the slight relative variations of RMS detected in that previous work. At the continuum level, the active region shows an abnormal granulation characterised by a σ_{Cont} value slightly smaller than for the quiet region, and at the MgIb₁ wing level, σ_{Mg} is smaller in the quiet region than in the active one. The behaviour of the RMS of the intensity variations

can also be qualitatively compared to numerical predictions of the RMS of the temperature variations. Gadun (1995) found the RMS of the temperature to decrease with increasing altitude in the atmosphere, while our results show an increase of the RMS of the intensity, for both quiet and active regions. Since this result is also valid for subsonically filtered data, *p*-modes, which are not taken into account in the simulations, cannot be responsible for this.

The spatial intensity correlation we observe between the continuum and the MgIb₁ line wing outside the active region can be compared to previous observations and models. The granulation contrast is predicted to show a reversing with increasing height. Following Gadun (1995), the intergranules will be brighter than the granules above a height $h \geq 190$ km. As the calculations of Stellmacher (private communication) place the MgI line wing at $h \approx 140$ km, our positive correlation is still coherent with that prediction. Recently, Espagnet et al. (1995) have observed at different positions along the profile of the NaD2 line, and have found a coherence of the intensities between the $h \approx 0$ km level and heights up to $h \approx 60$ to 90 km. However, as pointed out by these authors, previous works (e.g. Komm et al. 1990) have shown a coherence up to $h \approx 170$ km, a result which is consistent with ours.

One of the most striking result is certainly the *temporal* behaviour of the intensity correlation between the continuum and the MgI line wing in the quiet region. Our observations, based on non filtered, subsonically and supersonically filtered time sequences (see Fig. 4) suggest a simple interpretation: the acoustic oscillations induce simultaneous intensity variations at the two levels because they are evanescent waves, whereas the leading of MgI intensity over continuum may be ascribed to falling plasma motions, with which the correlated dark structures we observed in both continuum and magnesium images can be associated, due to their darkness possibly reflecting downdrafts. This could be compared to the numerical simulations performed by Rast (1995), showing that the photosphere is dominated by downflows. However, these simulated spatial scales are different of our observed ones. A simple calculation of the speed of the falling plasma from the observed time offset (see Fig. 4) gives a value of $v \approx 1.2$ km/s, which is coherent with the speed of downwards granular motions (Stix 1989).

The problem of radiative excess or deficit of magnetic elements has been addressed at the continuum level. We have studied the intensities in the active region, discarding pixels corresponding to the pores. The first result is qualitative: from our correlograms (Fig. 3), it becomes clear that the intensities variations versus height can be separated in two groups: one following the behaviour of the quiet region, and another characterised by higher brightness in the MgIb₁ wing, which in turn is related to higher value of the magnetic field. At the continuum level, these magnetic regions corresponds to areas darker than their surroundings (radiative deficit at the continuum level). However, we have checked the contrast of these magnetic elements *outside* the active region, and surprisingly enough, they show a positive contrast (radiative excess at the continuum level), in agreement with Keller & Koutchmy (1991), which indicates

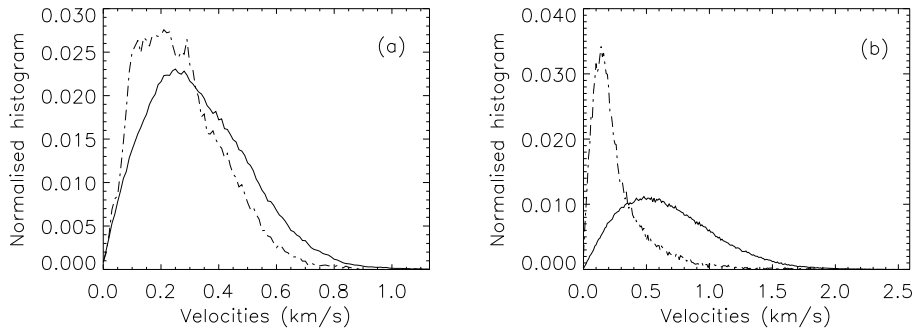


Fig. 7a and b. Histogram (normalised to the total number of counts in each region) of the horizontal velocities calculated in Section 3.3, at the continuum level (a) and at the MgIb₁ level (b) for the quiet (solid) and the active (dot dashed) regions, showing strikingly different behaviours

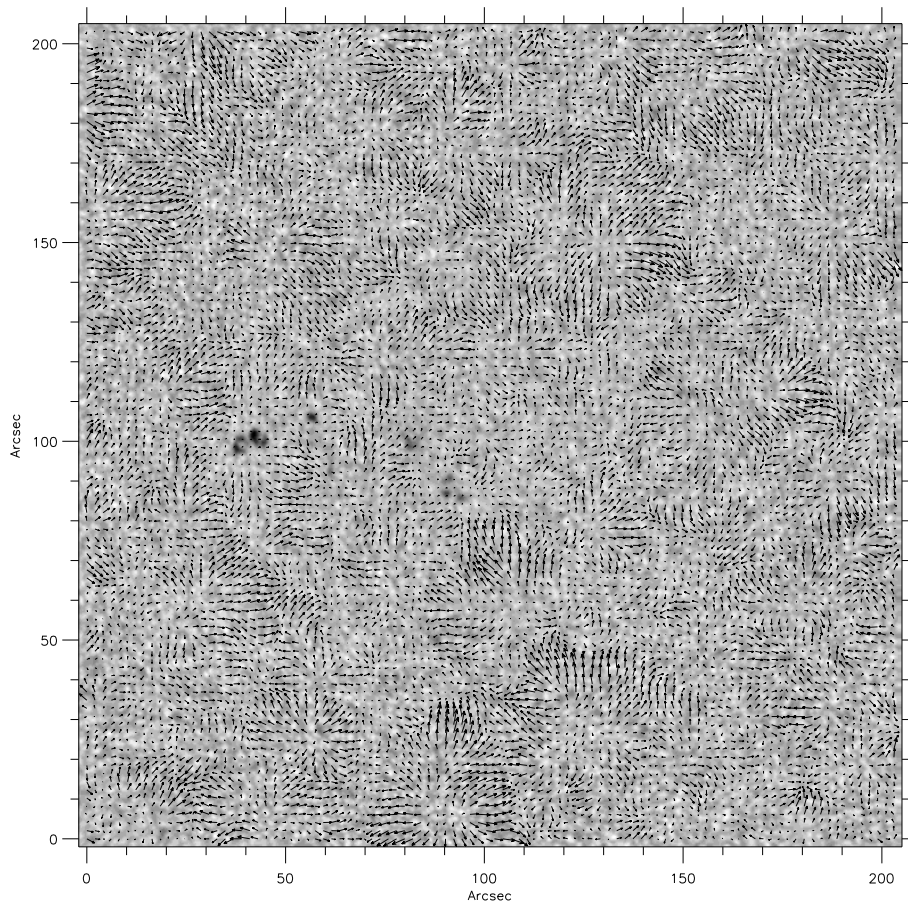


Fig. 8. Map of the horizontal velocity field at the continuum level plotted over a sample continuum image

that flux tubes inside an active region have a different behaviour than outside.

The remnant structure of the granulation we observed in the averaged continuum image may indicate a long life phenomenon in the granulation. Similar observation has been obtained by Hirzberger et al. (1997) as well. Considering the granulation at the surface of the sun as a randomly driven phenomenon with a typical lifetime of 5 mn leads to a number of approximately 22 “independent” realisations of the granular pattern during our 109 mn long sequence. Hence, we were expecting the residual RMS after averaging over the whole sequence to be about 0.6% (the RMS of single images divided by the square root of independent realisations). The fact that the observed RMS af-

ter averaging is two times greater suggests that the granulation should be described in a more complicated way, e.g. accounting for longer time scale phenomena.

Let us now discuss the behaviour of the horizontal motions of the plasma versus height and magnetic field. The first point is qualitative: the proper motions of the granules in the deep photosphere ($h \simeq 0$ km) show very clearly the supergranulation structure in the quiet region (see Fig. 8) and outlines clearly the magnetic network seen in the H α line (Fig. 10) which is also coincident with the bright points seen in the MgI line wing (see Baudin et al. 1996). This supergranular structure is not visible in the observed flows at the height of the MgIb₁ line wing ($h \simeq 140$ km, Fig. 9). The proper motions when observed in the active

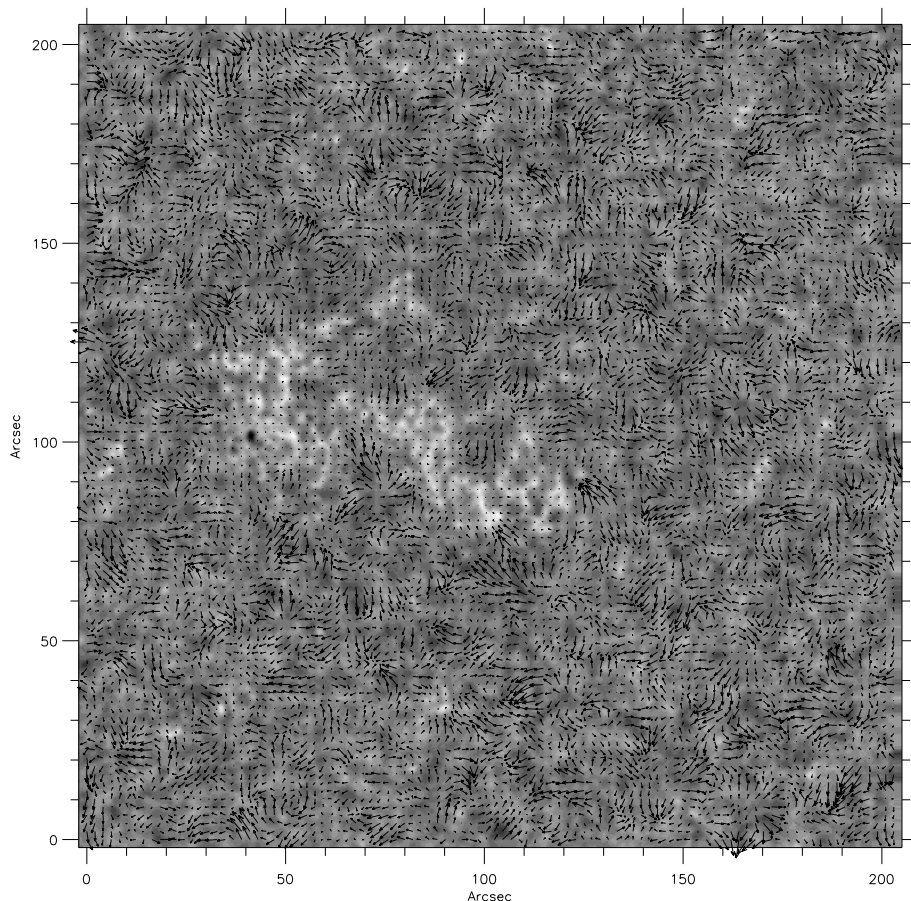


Fig. 9. Map of the horizontal velocity field at the MgIb₁ level, plotted over a sample MgIb₁ image

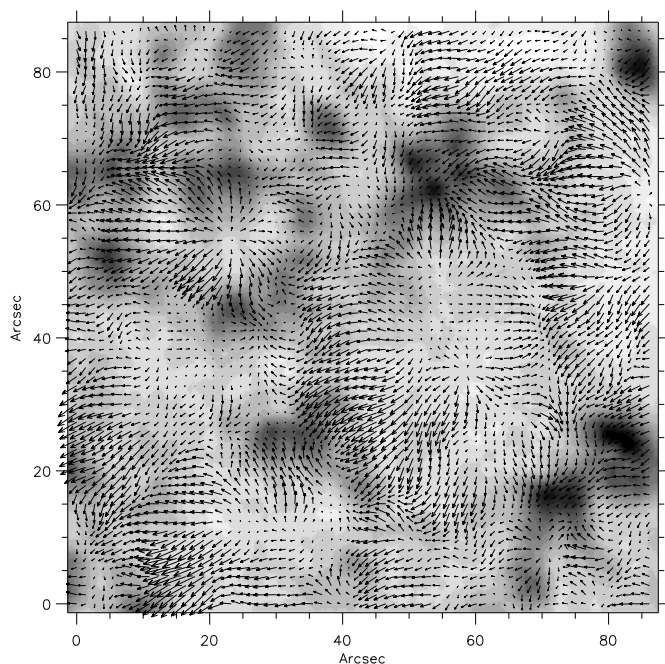


Fig. 10. Blow-up of the horizontal velocity field at the continuum level plotted over the H α (sum of the two wings) intensity map

and the quiet regions have a quite different behaviour. In the Q region, the averaged horizontal velocity is much higher at the MgI level ($h \simeq 140$ km) than at the continuum level ($h \simeq 0$ km): $\langle V_{Cont/Q} \rangle = 340$ m/s and $\langle V_{Mg/Q} \rangle = 680$ m/s. On the contrary, in the A region, averaged velocities are very similar: $\langle V_{Cont/A} \rangle = 270$ m/s and $\langle V_{Mg/A} \rangle = 280$ m/s. Moreover, the correlation coefficients of the components of the velocity vector at the two levels are much higher in the A region. This can be interpreted in a simple manner as a lower value of the parameter β of the plasma (i.e. the ratio of the gas pressure and magnetic pressure) which makes the plasma “frozen” in the magnetic region, specially at the MgI level.

There is a clear tendency for the bright points seen in the MgIb₁ images to appear at regions of photospheric flow convergence, which in turn outline the magnetic network (Simon et al. 1988, Wang et al. 1989). This may suggest that the flux tubes are then pushed and moved about towards the network by the velocity field, where they merge and concentrate.

Acknowledgements. We thank G. Stellmacher and R. Muller for their help and their comments on this work. The observations have been obtained at the VTT/SPO thanks to the excellent work provided by the staff there. Part of this work was made in the frame of the NATO CRG 940291, with the support of INSU and CNRS (France). FB and RMH have been supported by the Spanish DGICYT (project n^o 91-0530).

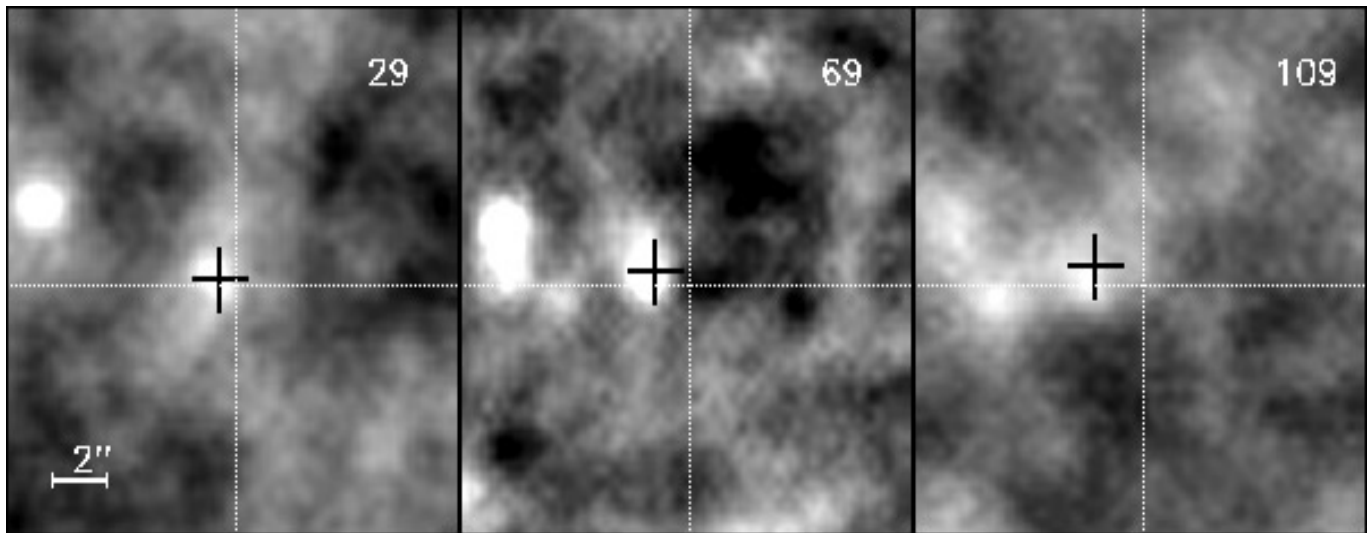


Fig. 11. Transverse displacement of a bright point during 109 min. Numbers on the upper right corner indicate minutes lasted since the beginning of the observations. Initial position of the bright point corresponds to the crossing point of the two thin dotted lines. The solid black cross represents the position of a test particle which is drifting with the photospheric flow field underneath. The scale of the figure in arcseconds is given by the solid bar on the lower left corner. The average velocity of this bright point is 220 m/s

References

- Baudin F., Bocchialini K., Koutchmy S., 1996, *A&A*, 314, L9
- Beckers J.M., 1976. In *Magnetic Fields in the Solar Atmosphere*, AFGL-TR-76-0131, Environmental Research Papers n° 568
- Chan K.L., Nordlung A., Steffen M., Stein R.F., 1991. In *Solar interior and atmosphere*, University of Arizona Press, p. 223
- Dara-Papamargaritis H., Koutchmy S., 1983, *A&A*, 125, 280
- Espagnet O., Muller R., Roudier T., Mein N., Mein P., 1995, *A&A Suppl. Ser.*, 109, 79
- Frazier E.N., 1970, *Solar Physics*, 14, 89
- Frazier E.N., 1971, *Solar Physics*, 21, 42
- Gadun A.S., 1995, *Kinematics and Physics of Celestial Bodies*, 11, No. 3, 54
- Hirzberger J., Vázquez M., Bonet J.A., Hanslmeier A., Sobotka M., 1997, *ApJ*, 480, 406
- Keller C.U., Koutchmy S., 1991, *Ap.J.*, 379, 751
- Komm R., Mattig W., Nesis A., 1990, *A&A*, 239, 340
- Koutchmy S., 1994 In *Infra-Red Solar Physics*, Proc. IAU Symp. 154, Dordrecht, Kluwer Academic Publisher, p. 239
- Koutchmy S., Lebecq C., 1986, *A&A*, 169, 323
- Molowny-Horas R., Yi Z., 1994, *Institute of Theoretical Astrophysics*, Internal Report n° 31
- November L.J., 1986, *Applied Optics*, 25, No. 3, 392
- Rast M.P., 1995, *Ap.J.*, 443, 863
- Rutten R. & Schrijver C. (eds), 1994, *Solar surface magnetism*, Kluwer Academic Publisher
- Stellmacher G., Wiehr E., 1991, *A&A*, 251, 675
- Stenflo J.O. (ed), 1990, *Solar Photosphere: Structure, Convection and Magnetic Fields*, Proc. IAU Symp. 138, Dordrecht, Kluwer Academic Publisher
- Simon G.W., Title A.M., Topka K.P., Tarbell T.D., Shine R.A., Ferguson S.H., Zirin H., and the SOUP Team, 1988, *Ap.J.*, 327, 964
- Stix M., 1989, *The Sun*, Springer-Verlag
- Title A.M., Tarbell T.D., Topka K.P., Ferguson S.H., Shine R.A. and the SOUP Team, 1989, *Ap. J.*, 336, 475
- Wang H., Tang F., Zirin H., Wang J., 1989, *Solar Phys.*, 165, 223
- Zhang Y., Engvold O., 1993, *Solar Phys.*, 144, 1